Research Article

Hui-Shen Shen*, Yang Xiang, and Yin Fan

Large amplitude vibration of doubly curved FG-GRC laminated panels in thermal environments

https://doi.org/10.1515/ntrev-2019-0042
Received Nov 24, 2019; accepted Dec 03, 2019

Abstract: A study on the large amplitude vibration of doubly curved graphene-reinforced composite (GRC) laminated panels is presented in this paper. A doubly curved panel is made of piece-wise GRC layers with functionally graded (FG) arrangement along the thickness direction of the panel. A GRC layer consists of polymer matrix reinforced by aligned graphene sheets. The material properties of the GRC layers are temperature dependent and can be estimated by the extended Halpin-Tsai micromechanical model. The modelling of the large amplitude vibration of the panels is based on the Reddy's higher order shear deformation theory and the effects of the von Kármán geometric nonlinearity, the panel-foundation interaction and the temperature variation are included in the derivation of the motion equations of the panels. The solutions for the large amplitude vibration of the doubly curved FG-GRC laminated panels are obtained by applying a two-step perturbation approach. A parametric study is carried out to determine the influences of foundation stiffness, temperature variation, FG distribution pattern, in-plane boundary condition and panel curvature ratio on the natural frequencies and the nonlinear to linear frequency ratios of the doubly curved FG-GRC laminated panels.

Keywords: Nanocomposites; Functionally graded materials; Temperature-dependent properties

1 Introduction

Doubly curved panels have many important engineering applications. During their service life, these panels may be subjected to different combinations of loading and environmental conditions which can cause the panels to experience large amplitude vibration with the panel deflection being in the order of the panel thickness. Therefore, it is necessary to fully understand the nonlinear vibration behaviors of doubly curved panels in thermal environments in engineering design and practice. Many studies have been carried out on the nonlinear vibration behavior of isotropic and composite laminated curved panels [1–8]. It is observed that an acceptable agreement for flat plates can be achieved by different researchers. However, the results for a curved panel exist large discrepancies which may be due to the hardening behavior (*i.e.* increase in vibration amplitude leads to the increase of the nonlinear frequency) or the softening behavior of the panel (*i.e.* increase in vibration amplitude leads to the decrease of the nonlinear frequency) [1–8].

Advanced composite materials possess unique features that many of the conventional materials do not have. We have witnessed the increased use of advanced composite materials, including the functionally graded material (FGM) [9], as key structural members in various engineering applications. Shen [10] first proposed to use FGM concept to nanocomposite structures in order to fully utilize the effect of nano filler reinforcement in composite structures. Shen and his co-authors and other research teams further studied the linear and nonlinear vibration characteristics of FGM curved panels [11–17] and FG carbon nanotube reinforced composite (CNTRC) curved panels [18–22] subject to temperature changes and/or resting on elastic foundations. Since the discovery of graphene by Geim and Novoselov in 2004 [23], extensive studies on graphene have been conducted by many researchers and the extraordinary material properties of graphene have been widely reported [24–28]. Due to these remarkable properties, graphene has become one of the ideal reinforcement agents in creating advanced polymer composites [29]. For graphene-based nanocomposites, one kind

***Corresponding Author: Hui-Shen Shen:** School of Aeronautics and Astronautics, School of Ocean and Civil Engineering, Shanghai Jiao Tong University, Shanghai 200240, China;
Email: hsshen@sjtu.edu.cn
Yang Xiang: School of Engineering, Western Sydney University, Locked Bag 1797, Penrith, NSW 2751, Australia
Yin Fan: Department of Aerospace Engineering, Mississippi State University, Mississippi State, MS 39762, United States of America

is graphene platelet reinforced composite (GPLRC) where both the polymer matrix and graphene platelets (GPLs) are assumed to be isotropic and independent of temperature. In essence, GPL reinforced composites belong to particle reinforced composites. The GPLRC model is relatively simple and was adopted by many researchers, for example, the vibration analysis for doubly-curved panels reinforced by GPLs was reported by Wang *et al.* [30, 31] and Fazelzadeh *et al.* [32]. It is noted that graphene sheets have anisotropic and temperature dependent material properties [24–28] and it is possible to align graphene sheets in polymer matrix that can result in better reinforcement effect for the graphene-based composites [33–35]. Shen *et al.* [36] first proposed a functionally graded graphene reinforced composite (GRC) model where aligned graphene reinforcements are anisotropic and the material properties of both the polymer matrix and graphene sheets are assumed to be temperature dependent. As reported by Lei *et al.* [37] the GRC model is more accurate than GPLRC model and was adopted by many researchers [38–43].

This paper will investigate the nonlinear free vibration behavior of doubly curved GRC laminated panels resting on elastic foundations in thermal environments. The panels with the piece-wise functionally graded GRC laminar layer pattern are considered in the study. The novelty of this study lies in the account of both the functionally graded material configurations and the temperature dependent properties in the nonlinear vibration analyses of FG-GRC laminated doubly curved panels. The extended Halpin-Tsai micromechanical model is applied to estimate the material properties of the GRC layers. The Reddy's third order shear deformation shell theory is employed to derive the motion equations for the GRC laminated panels. Note that the motion equations of the panels also include the effects of the von Kármán geometric nonlinearity, the foundation support and the temperature variation. The boundary conditions of the panels are assumed to be simply supported. A two-step perturbation approach is employed to determine the nonlinear frequencies of doubly curved GRC laminated panels. The large amplitude vibration behavior of doubly curved FG-GRC laminated panels subject to the influence of foundation support and temperature variation is discussed in detail.

2 Large amplitude vibration of doubly curved GRC laminated panels

A doubly curved GRC laminated panel with two radii of curvature R_1 and R_2, as shown in Figure 1, is considered in this study. The panel is made of N laminated GRC layers of different graphene volume fractions to form five different functionally graded (FG) patterns, *i.e.* UD, FG-Λ, FG-V, FG-X and FG-O. The panel with the UD pattern consists of GRC layers of the same graphene volume fraction. The panel with the FG-O pattern has the maximum graphene volume fraction in the GRC layers at the mid-plane and the minimum graphene volume fraction at the top and bottom GRC layers with a step change of graphene volume fractions between the surface and the mid-plane GRC layers, while the panel with the FG-X pattern has an inverse graphene volume fraction arrangement as that of the FG-O pattern. The FG-V panel consists of graphene-rich top GRC layers and graphene-poor bottom GRC layer, while the FG-Λ panel has an inverse graphene volume fraction arrangement as that of the FG-V panel. The panel has length a, width b and thickness h and is located in a coordinate system (X, Y, Z) as shown in Figure 1. Note that X and Y are in the directions of the curvature lines on the middle surface of the panel and Z is in the direction of the inward normal to the middle surface of the panel. The panel is supported by a Pasternak-type foundation with the panel-foundation pressure being defined by $p_0 = \overline{K}_1\overline{W} - \overline{K}_2\nabla^2\overline{W}$, where $\overline{W}$ is the displacement of the panel in the Z direction, $\overline{K}_1$ is the transverse foundation stiffness (Winkler stiffness) and $\overline{K}_2$ is the shearing layer stiffness of the foundation, and $\nabla^2 = \partial^2/\partial X^2 + \partial^2/\partial Y^2$ is the Laplace operator.

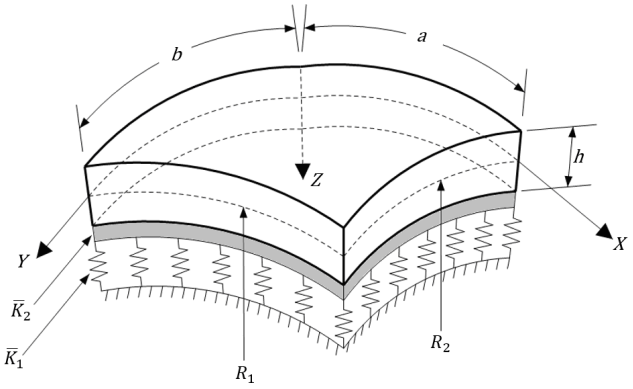

Figure 1: Coordinate system and geometry for a doubly curved panel supported by a Pasternak-type elastic foundation

One of the key issues in structural analysis of graphene reinforced composites is the thermomechanical property evaluation of the composite. The Halpin-Tsai micromechanical model [44] is employed to estimate the effective material properties of the GRC layers in this study as we assume that the graphene sheets are aligned in the polymer matrix to form aligned 2D reinforcement agents. Due to incomplete stress transfer between graphene sheets and polymer matrix resulting from surface effect, strain gradients effect and intermolecular effect, the Halpin-Tsai model needs to be modified to account for these effects [45]. In the present study, the graphene reinforcement is either zigzag (refer to as 0-ply) or armchair (refer to as 90-ply). Based on the extended Halpin-Tsai model, the effective Young's moduli and the shear modulus of the GRC layer can be expressed as [36]

$$E_{11} = \eta_1 \frac{1 + 2(a_G/h_G)\gamma_{11}^G V_G}{1 - \gamma_{11}^G V_G} E^m \tag{1a}$$

$$E_{22} = \eta_2 \frac{1 + 2(b_G/h_G)\gamma_{22}^G V_G}{1 - \gamma_{22}^G V_G} E^m \tag{1b}$$

$$G_{12} = \eta_3 \frac{1}{1 - \gamma_{12}^G V_G} G^m \tag{1c}$$

in which a_G, b_G and h_G are the length, the width and the effective thickness of the graphene sheet, and

$$\gamma_{11}^G = \frac{E_{11}^G/E^m - 1}{E_{11}^G/E^m + 2a_G/h_G} \tag{2a}$$

$$\gamma_{22}^G = \frac{E_{22}^G/E^m - 1}{E_{22}^G/E^m + 2b_G/h_G} \tag{2b}$$

$$\gamma_{12}^G = \frac{G_{12}^G/G^m - 1}{G_{12}^G/G^m} \tag{2c}$$

where E^m and G^m are the elasticity modulus and shear modulus of the polymer matrix. Besides, E_{11}^G, E_{22}^G and G_{12}^G indicate the elasticity moduli and shear modulus of graphene sheet. We can see that the only difference between Eq. (1) and the conventional Halpin-Tsai model is the presence of efficiency parameters η_j (j=1,2,3). These parameters are obtained by matching the data which are evaluated by MD simulations [46] and the Halpin-Tsai model. In Eq. (1), V_G and V_m are the volume fractions of graphene and matrix, which should satisfy the partition of unity condition $V_G + V_m = 1$.

Poisson's ratio ν_{12} and the mass density ρ of the GRC layer may easily be expressed according to the conventional rule of mixtures

$$\begin{bmatrix} \nu_{12} \\ \rho \end{bmatrix} = \begin{bmatrix} \nu_{12}^G & \nu^m \\ \rho^G & \rho^m \end{bmatrix} \begin{bmatrix} V_G \\ V_m \end{bmatrix} \tag{3}$$

where ν_{12}^G, ρ^G and ν^m, ρ^m are the Poisson's ratios and mass densities of the graphene and matrix, respectively. They are assumed to be weakly dependent on temperature variation.

Note that the material properties of the GRC layers estimated in Eq. (1) are temperature dependent as the material properties of the graphene sheets and the polymer matrix are both temperature dependent. According to Schapery model [47], the thermal expansion coefficients of the GRC layers can be expressed by

$$\alpha_{11} = \frac{V_G E_{11}^G \alpha_{11}^G + V_m E^m \alpha^m}{V_G E_{11}^G + V_m E^m} \tag{4a}$$

$$\alpha_{22} = (1 + \nu_{12}^G) V_G \alpha_{22}^G + (1 + \nu^m) V_m \alpha^m - \nu_{12} \alpha_{11} \tag{4b}$$

in which α_{11} and α_{22} are the longitudinal and transverse thermal expansion coefficients of the GRC layers, α_{11}^G, α_{22}^G and α^m are thermal expansion coefficients, respectively, of the graphene and matrix.

The doubly curved GRC laminated panel is subjected to a transverse dynamic load $q(X, Y, \bar{t})$ in a thermal environment. Within the framework of the Reddy's third order shear deformation shell theory [48] and considering the effects of the von Kármán geometric nonlinearity, the panel-foundation interaction and the temperature variation, we can derive the motion equations for the doubly curved panel as follows

$$\begin{aligned} &\tilde{L}_{11}(\overline{W}) - \tilde{L}_{12}(\overline{\Psi}_x) - \tilde{L}_{13}(\overline{\Psi}_y) + \tilde{L}_{14}(\overline{F}) - \tilde{L}_{15}(\overline{N}^T) \\ &- \tilde{L}_{16}(\overline{M}^T) - \frac{1}{R_1}\overline{F}_{,YY} - \frac{1}{R_2}\overline{F}_{,XX} + (\overline{K}_1 \overline{W} - \overline{K}_2 \nabla^2 \overline{W}) \\ &= \tilde{L}(\overline{W}, \overline{F}) + \tilde{L}_{17}\left(\frac{\partial^2 \overline{W}}{\partial \bar{t}^2}\right) - \left(\tilde{I}_5 \frac{\partial^3 \overline{\Psi}_x}{\partial X \partial \bar{t}^2} + \tilde{I}_5' \frac{\partial^3 \overline{\Psi}_y}{\partial Y \partial \bar{t}^2}\right) + q \end{aligned} \tag{5}$$

$$\begin{aligned} &\tilde{L}_{21}(\overline{F}) + \tilde{L}_{22}(\overline{\Psi}_x) + \tilde{L}_{23}(\overline{\Psi}_y) - \tilde{L}_{24}(\overline{W}) - \tilde{L}_{25}(\overline{N}^T) \\ &+ \frac{1}{R_1}\overline{W}_{,YY} + \frac{1}{R_2}\overline{W}_{,XX} = -\frac{1}{2}\tilde{L}(\overline{W}, \overline{W}) \end{aligned} \tag{6}$$

$$\begin{aligned} &\tilde{L}_{31}(\overline{W}) + \tilde{L}_{32}(\overline{\Psi}_x) - \tilde{L}_{33}(\overline{\Psi}_y) + \tilde{L}_{34}(\overline{F}) - \tilde{L}_{35}(\overline{N}^T) \\ &- \tilde{L}_{36}(\overline{S}^T) = \hat{I}_5 \frac{\partial^3 \overline{W}}{\partial X \partial \bar{t}^2} - \hat{I}_3 \frac{\partial^2 \overline{\Psi}_x}{\partial \bar{t}^2} \end{aligned} \tag{7}$$

$$\begin{aligned} &\tilde{L}_{41}(\overline{W}) - \tilde{L}_{42}(\overline{\Psi}_x) + \tilde{L}_{43}(\overline{\Psi}_y) + \tilde{L}_{44}(\overline{F}) - \tilde{L}_{45}(\overline{N}^T) \\ &- \tilde{L}_{46}(\overline{S}^T) = \hat{I}_5' \frac{\partial^3 \overline{W}}{\partial Y \partial \bar{t}^2} - \hat{I}_3 \frac{\partial^2 \overline{\Psi}_y}{\partial \bar{t}^2} \end{aligned} \tag{8}$$

in which

$$\tilde{L}_{17}(\ ) = -I_1 - \left(\tilde{I}_7 \frac{\partial^2}{\partial X^2} + \tilde{I}_7' \frac{\partial^2}{\partial Y^2}\right) \tag{9}$$

where a comma denotes partial differentiation with respect to the corresponding coordinates, and $\overline{W}$ is the transverse displacement, $\overline{\Psi}_x$ and $\overline{\Psi}_y$ are the rotations of the normals to the middle surface with respect to the Y - and X - axes, $\overline{F}$ is the stress function defined by $\overline{N}_x = \partial^2\overline{F}/\partial Y^2$, $\overline{N}_y = \partial^2\overline{F}/\partial X^2$ and $\overline{N}_{xy} = -\partial^2\overline{F}/\partial X\partial Y$. $\tilde{L}_{ij}(\,)$ and $\tilde{L}(\,)$ are the linear and nonlinear operators as defined in Shen [49], and $\tilde{L}(\,)$ contains the geometric nonlinearity terms in the von Kármán sense, and can be given by

$$\tilde{L}(\,) = \frac{\partial^2}{\partial X^2}\frac{\partial^2}{\partial Y^2} - 2\frac{\partial^2}{\partial X\partial Y}\frac{\partial^2}{\partial X\partial Y} + \frac{\partial^2}{\partial Y^2}\frac{\partial^2}{\partial X^2} \tag{10}$$

The panel is assumed to be in a constant temperature field at an isothermal state. The terms associated with the superscript T in Eqs. (5)-(8) contain the effect of temperature variation, $\overline{N}^T$ are the thermal forces, $\overline{M}^T$ are the thermal moments and $\overline{P}^T$ are the higher order thermal moments. The effect of the panel-foundation interaction is included in the terms associated with $\overline{K}_1$ and $\overline{K}_2$ in Eq. (5). The terms I_j, $\hat{I}_j$ and $\tilde{I}_j$ as well as $\overline{N}^T$, $\overline{M}^T$ and $\overline{P}^T$ are given in detail in Appendix A. We can use Eqs. (5)-(8) to analyse the case for GRC laminated cylindrical panels by setting $R_2 = R$ and $R_1 = \infty$ and for GRC laminated square spherical panels by setting $R_1 = R_2 = R$.

Besides the governing equations (5)-(8), it is necessary to deal with different boundary conditions to solve the boundary-value problem. In the current study, the four curved edges of the panel are assumed to be simply supported, and the associate boundary conditions are

$$\overline{W} = \overline{\Psi}_y = \overline{M}_x = \overline{P}_x = 0 \quad (\text{at } X = 0, a) \tag{11a}$$

$$\overline{W} = \overline{\Psi}_x = \overline{M}_y = \overline{P}_y = 0 \quad (\text{at } Y = 0, b) \tag{11b}$$

where $\overline{M}_x$ and $\overline{M}_y$ are the bending moments and $\overline{P}_x$ and $\overline{P}_y$ are the higher order moments as defined in Reddy and Liu [48].

Two in-plane boundary conditions, *i.e.* movable and immovable, are considered. For movable in-plane boundary conditions, one has

$$\overline{N}_x = 0 \quad (\text{at } X = 0, a) \tag{11c}$$

$$\overline{N}_y = 0 \quad (\text{at } Y = 0, b) \tag{11d}$$

and for immovable in-plane boundary conditions, one has

$$\overline{U} = 0 \quad (\text{at } X = 0, a) \tag{11e}$$

$$\overline{V} = 0 \quad (\text{at } Y = 0, b) \tag{11f}$$

where $\overline{U}$ and $\overline{V}$ are the plate displacements in the X and Y directions.

The movable conditions of Eqs. (11c) and (11d) can be imposed in the average sense as

$$\int_0^b \overline{N}_x dY = 0, \quad \int_0^a \overline{N}_y\, dX = 0 \tag{12}$$

Also, the immovable conditions of Eqs. (11e) and (11f) are fulfilled in the average sense as

$$\int_0^b\int_0^a \frac{\partial\overline{U}}{\partial X}dXdY = 0, \quad \int_0^a\int_0^b \frac{\partial\overline{V}}{\partial Y}dYdX = 0 \tag{13}$$

or

$$\begin{aligned}\int_0^b\int_0^a \Bigg[&\left(A_{11}^\star\frac{\partial^2\overline{F}}{\partial Y^2} + A_{12}^\star\frac{\partial^2\overline{F}}{\partial X^2}\right) \\ &+ \left(B_{11}^\star - \frac{4}{3h^2}E_{11}^\star\right)\frac{\partial\overline{\Psi}_x}{\partial X} + \left(B_{12}^\star - \frac{4}{3h^2}E_{12}^\star\right)\frac{\partial\overline{\Psi}_y}{\partial Y} \\ &- \frac{4}{3h^2}\left(E_{11}^\star\frac{\partial^2\overline{W}}{\partial X^2} + E_{12}^\star\frac{\partial^2\overline{W}}{\partial Y^2}\right) + \frac{\overline{W}}{R_1} - \frac{1}{2}\left(\frac{\partial\overline{W}}{\partial X}\right)^2 \\ &- \left(A_{11}^\star\overline{N}_x^T + A_{12}^\star\overline{N}_y^T\right)\Bigg]dXdY = 0\end{aligned} \tag{14a}$$

$$\begin{aligned}\int_0^a\int_0^b \Bigg[&\left(A_{22}^\star\frac{\partial^2\overline{F}}{\partial X^2} + A_{12}^\star\frac{\partial^2\overline{F}}{\partial Y^2}\right) \\ &+ \left(B_{21}^\star - \frac{4}{3h^2}E_{21}^\star\right)\frac{\partial\overline{\Psi}_x}{\partial X} + \left(B_{22}^\star - \frac{4}{3h^2}E_{22}^\star\right)\frac{\partial\overline{\Psi}_y}{\partial Y} \\ &- \frac{4}{3h^2}\left(E_{21}^\star\frac{\partial^2\overline{W}}{\partial X^2} + E_{22}^\star\frac{\partial^2\overline{W}}{\partial Y^2}\right) + \frac{\overline{W}}{R_2} \\ &- \frac{1}{2}\left(\frac{\partial\overline{W}}{\partial Y}\right)^2 - \left(A_{12}^\star\overline{N}_x^T + A_{22}^\star\overline{N}_y^T\right)\Bigg]dYdX = 0\end{aligned} \tag{14b}$$

In the above equations, the reduced stiffness matrices $[A_{ij}^\star]$, $[B_{ij}^\star]$, $[D_{ij}^\star]$, $[E_{ij}^\star]$, $[F_{ij}^\star]$ and $[H_{ij}^\star]$ are defined in Appendix B.

It should be noticed that, in the current study, either governing equations (5)-(8) or boundary conditions (11a)-(11f) are different from that used in [50]. For nonlinear problems the superposition principle is no longer valid. Hence, each nonlinear boundary value problem with different governing equations or boundary conditions should be solved separately.

3 Solution procedure

The nonlinear vibrations of flat or cylindrical or doubly curved panels are different nonlinear problems. A two-step perturbation approach was developed by Shen [49]

and was successfully to solve different kinds of nonlinear problems of beams, plates and shells by many research teams [51–61]. To use this two-step perturbation approach to solve the large amplitude vibration problem of doubly curved FG-GRC laminated panels, the motion equations (5) to (8) can be expressed in dimensionless forms as

$$\begin{aligned} &L_{11}(W) - L_{12}(\Psi_x) - L_{13}(\Psi_y) + \gamma_{14} L_{14}(F) - L_{16}(M^T) \\ &- \eta^{-1}\gamma_{14} F,_{xx} - \eta^{-1}\gamma_0\gamma_{14}\beta^2 F,_{yy} + (K_1 W - K_2\nabla^2 W) \\ &= \gamma_{14}\beta^2 L(W,F) + L_{17}\left(\frac{\partial^2 W}{\partial t^2}\right) \\ &+ \left(\gamma_{81}\frac{\partial^3 \Psi_x}{\partial x \partial t^2} + \gamma_{82}\beta\frac{\partial^3 \Psi_y}{\partial y \partial t^2}\right) + \lambda_q \end{aligned} \tag{15}$$

$$\begin{aligned} &L_{21}(F) + \gamma_{24} L_{22}(\Psi_x) + \gamma_{24} L_{23}(\Psi_y) - \gamma_{24} L_{24}(W) \\ &+ \eta^{-1}\gamma_{24} W,_{xx} + \eta^{-1}\gamma_0\gamma_{24}\beta^2 W,_{yy} = -\frac{1}{2}\gamma_{24}\beta^2 L(W,W) \end{aligned} \tag{16}$$

$$\begin{aligned} &L_{31}(W) + L_{32}(\Psi_x) - L_{33}(\Psi_y) + \gamma_{14} L_{34}(F) - L_{36}(S^T) \\ &= \gamma_{83}\frac{\partial^3 W}{\partial x \partial t^2} + \gamma_{91}\frac{\partial^2 \Psi_x}{\partial t^2} \end{aligned} \tag{17}$$

$$\begin{aligned} &L_{41}(W) - L_{42}(\Psi_x) + L_{43}(\Psi_y) + \gamma_{14} L_{44}(F) - L_{46}(S^T) \\ &= \gamma_{84}\beta\frac{\partial^3 W}{\partial y \partial t^2} + \gamma_{92}\frac{\partial^2 \Psi_y}{\partial t^2} \end{aligned} \tag{18}$$

with

$$L_{17}(\,) = \gamma_{170} + \left(\gamma_{171}\frac{\partial^2}{\partial x^2} + \gamma_{172}\beta^2\frac{\partial^2}{\partial y^2}\right) \tag{19}$$

and the other dimensionless linear operators $L_{ij}(\,)$ are given in Shen [49]. In Eqs. (15)-(19), the non-dimensional parameters are defined by

$$\begin{aligned} &x = \pi\frac{X}{a}, \quad y = \pi\frac{Y}{b}, \quad \beta = \frac{a}{b}, \\ &\eta = \frac{\pi^2 R_2}{a^2}[D_{11}^* D_{22}^* A_{11}^* A_{22}^*]^{1/4}, \quad \gamma_0 = \frac{R_2}{R_1}, \\ &W = \frac{\overline{W}}{[D_{11}^* D_{22}^* A_{11}^* A_{22}^*]^{1/4}}, \\ &(\Psi_x, \Psi_y) = \frac{a}{\pi}\frac{(\overline{\Psi}_x, \overline{\Psi}_y)}{[D_{11}^* D_{22}^* A_{11}^* A_{22}^*]^{1/4}}, \quad F = \frac{\overline{F}}{[D_{11}^* D_{22}^*]^{1/2}}, \\ &(M_x,\ P_x) = \frac{a^2}{\pi^2}\frac{1}{D_{11}^*[D_{11}^* D_{22}^* A_{11}^* A_{22}^*]^{1/4}}\left(\overline{M}_x,\ \frac{4}{3h^2}\overline{P}_x\right), \\ &t = \frac{\pi\bar{t}}{a}\sqrt{\frac{E_0}{\rho_0}}, \quad \omega_L = \Omega_L\frac{a}{\pi}\sqrt{\frac{\rho_0}{E_0}}, \quad \gamma_{14} = \left[\frac{D_{22}^*}{D_{11}^*}\right]^{1/2}, \\ &\gamma_{24} = \left[\frac{A_{11}^*}{A_{22}^*}\right]^{1/2}, \quad \gamma_5 = -\frac{A_{12}^*}{A_{22}^*}, \\ &(\gamma_{T1}, \gamma_{T2}) = (A_x^T,\ A_y^T)R_2\left[\frac{A_{11}^* A_{22}^*}{D_{11}^* D_{22}^*}\right]^{1/4}, \end{aligned} \tag{20}$$

$$\begin{aligned} &(\gamma_{T4}, \gamma_{T5}, \gamma_{T7}, \gamma_{T8}) = \frac{a^2}{\pi^2 h D_{11}^*}(D_x^T,\ D_y^T,\ \frac{4}{3h^2}F_x^T,\ \frac{4}{3h^2}F_y^T), \\ &\gamma_{170} = -\frac{I_1 E_0 a^2}{\pi^2\rho_0 D_{11}^*}, \\ &(\gamma_{91},\ \gamma_{92}, \gamma_{81},\ \gamma_{82},\ \gamma_{83},\ \gamma_{84},\ \gamma_{171}, \gamma_{172}) \\ &= (-\hat{I}_3,\ -\hat{I}_3',\ -\tilde{I}_5,\ -\tilde{I}_5',\ \hat{I}_5,\ \hat{I}_5',\ -\tilde{I}_7,\ -\tilde{I}_7')\frac{E_0}{\rho_0 D_{11}^*}, \\ &(K_1, k_1) = \overline{K}_1\left(\frac{a^4}{\pi^4 D_{11}^*},\ \frac{b^4}{E_0 h^3}\right), \\ &(K_2, k_2) = \overline{K}_2\left(\frac{a^2}{\pi^2 D_{11}^*},\ \frac{b^2}{E_0 h^3}\right), \\ &\lambda_q = \frac{qa^4}{\pi^4 D_{11}^*[D_{11}^* D_{22}^* A_{11}^* A_{22}^*]^{1/4}}, \end{aligned}$$

in which E_0 and ρ_0 are the material properties of the polymer matrix E^m and ρ^m at room temperature (T_0=300 K), and the terms A_x^T, D_x^T, F_x^T, etc. are defined by

$$\begin{aligned} &\begin{bmatrix} A_x^T & D_x^T & F_x^T \\ A_y^T & D_y^T & F_y^T \end{bmatrix}\Delta T \\ &= -\sum_{k=1}^{N}\int_{h_{k-1}}^{h_k}\begin{bmatrix} A_x \\ A_y \end{bmatrix}(1, Z, Z^3)\Delta T dZ \end{aligned} \tag{21}$$

Based on Eq. (20), the boundary conditions of Eqs. (11a) and (11b) can be written in non-dimensional forms as

$$W = \Psi_y = M_x = P_x = 0 \quad (\text{at } x = 0, \pi) \tag{22a}$$

$$W = \Psi_x = M_y = P_y = 0 \quad (\text{at } y = 0, \pi) \tag{22b}$$

and the movable in-plane boundary conditions of Eqs. (11c) and (11d) become

$$\int_0^{\pi}\frac{\partial^2 F}{\partial y^2}dy = 0 \quad (\text{at } x = 0, \pi) \tag{22c}$$

$$\int_0^{\pi}\frac{\partial^2 F}{\partial x^2}dx = 0 \quad (\text{at } y = 0, \pi) \tag{22d}$$

and the immovable in-plane boundary conditions of Eqs. (11e) and (11f) become

$$\begin{aligned} &\int_0^{\pi}\int_0^{\pi}\left[\left(\gamma_{24}^2\beta^2\frac{\partial^2 F}{\partial y^2} - \gamma_5\frac{\partial^2 F}{\partial x^2}\right)\right. \\ &+ \gamma_{24}\left(\gamma_{511}\frac{\partial \Psi_x}{\partial x} + \gamma_{233}\beta\frac{\partial \Psi_y}{\partial y}\right) \\ &- \gamma_{24}\left(\gamma_{611}\frac{\partial^2 W}{\partial x^2} + \gamma_{244}\beta^2\frac{\partial^2 W}{\partial y^2}\right) + \eta^{-1}\gamma_0\gamma_{24}W \end{aligned} \tag{22e}$$

$$-\frac{1}{2}\gamma_{24}\left(\frac{\partial W}{\partial x}\right)^2+\eta^{-1}(\gamma_{24}^2\gamma_{T1}-\gamma_5\gamma_{T2})\Delta T\Bigg]dxdy=0$$

(at $x=0,\pi$)

$$\int_0^{\pi}\int_0^{\pi}\Bigg[\left(\frac{\partial^2 F}{\partial x^2}-\gamma_5\beta^2\frac{\partial^2 F}{\partial y^2}\right) \tag{22f}$$
$$+\gamma_{24}\left(\gamma_{220}\frac{\partial \Psi_x}{\partial x}+\gamma_{522}\beta\frac{\partial \Psi_y}{\partial y}\right)$$
$$-\gamma_{24}\left(\gamma_{240}\frac{\partial^2 W}{\partial x^2}+\gamma_{622}\beta^2\frac{\partial^2 W}{\partial y^2}\right)+\eta^{-1}\gamma_{24}W$$
$$-\frac{1}{2}\gamma_{24}\beta^2\left(\frac{\partial W}{\partial y}\right)^2+\eta^{-1}(\gamma_{T2}-\gamma_5\gamma_{T1})\Delta T\Bigg]dydx=0$$

(at $y=0,\pi$)

where γ_{ijk} are defined in Shen [49].

Equations (15) to (18) can be separated into two sets of differential equations which are then solved in sequence. The first set of differential equations is for the nonlinear thermal bending problem and can be solved using the same method as reported in [62], and the second set of differential equations are used to obtain the homogeneous vibration solution on the initial deflected panel. A two-step perturbation technique is applied to determine this homogeneous solution. We assume that the perturbation equations for the displacements and the forces with a small perturbation parameter ε which has no physical meaning in the first step are given by

$$\begin{aligned}
W(x,y,\tau,\varepsilon)&=\sum_{j=1}\varepsilon^j w_j(x,y,\tau), \qquad (23)\\
\Psi_x(x,y,\tau,\varepsilon)&=\sum_{j=1}\varepsilon^j \Psi_{xj}(x,y,\tau),\\
\Psi_y(x,y,\tau,\varepsilon)&=\sum_{j=1}\varepsilon^j \Psi_{yj}(x,y,\tau),\\
F(x,y,\tau,\varepsilon)&=\sum_{j=0}\varepsilon^j f_j(x,y,\tau),\\
\lambda_q(x,y,\tau,\varepsilon)&=\sum_{j=1}\varepsilon^j \lambda_j(x,y,\tau),
\end{aligned}$$

We introduce $\tau=\varepsilon t$ to improve the perturbation solution process for solving the large amplitude vibration problem. In order to satisfy the simply supported boundary conditions in the space domain, the first order solution of the panel is assumed to have the form

$$w_1(x,y,\tau)=A_{11}^{(1)}(\tau)\sin mx\sin ny \tag{24}$$

where (m, n) is the number of waves of vibration mode in the X and Y directions. The initial conditions are assumed to be

$$W|_{t=0}=\frac{\partial W}{\partial t}|_{t=0}=0,\quad \Psi_x|_{t=0}=\frac{\partial \Psi_x}{\partial t}|_{t=0}=0, \tag{25}$$
$$\Psi_y|_{t=0}=\frac{\partial \Psi_y}{\partial t}|_{t=0}=0$$

Taking into consideration of Eq. (23), a set of perturbation equations are obtained by collecting the terms of the same order of ε in Eqs. (15)-(18). Eq. (24) is then applied as the first step solution to the perturbation equations and following a step by step approach, we can obtain the 4^{th} order asymptotic solutions as

$$\begin{aligned}
W(x,y,t)&=\varepsilon A_{11}^{(1)}(t)\sin mx\sin ny \qquad (26)\\
&\quad+(\varepsilon A_{11}^{(1)}(t))^3[a_{331}\sin 3mx\sin ny\\
&\quad+a_{313}\sin mx\sin 3ny]+O(\varepsilon^4)
\end{aligned}$$

$$\begin{aligned}
\Psi_x(x,y,t)&=\left[(\varepsilon A_{11}^{(1)}(t))c_{111}+\left(\varepsilon\frac{\partial^2 A_{11}^{(1)}(t)}{\partial t^2}\right)c_{311}\right] \qquad (27)\\
&\quad\cdot\cos mx\sin ny+(\varepsilon A_{11}^{(1)}(t))^3\\
&\quad[c_{331}\cos 3mx\sin ny+c_{313}\cos mx\sin 3ny]\\
&\quad+O(\varepsilon^4)
\end{aligned}$$

$$\begin{aligned}
\Psi_y(x,y,t)&=\left[(\varepsilon A_{11}^{(1)}(t))d_{111}+\left(\varepsilon\frac{\partial^2 A_{11}^{(1)}(t)}{\partial t^2}\right)d_{311}\right] \qquad (28)\\
&\cdot\sin mx\cos ny+(\varepsilon A_{11}^{(1)}(t))^3[d_{331}\sin 3mx\cos ny\\
&+d_{313}\sin mx\cos 3ny]+O(\varepsilon^4)
\end{aligned}$$

$$\begin{aligned}
F(x,y,t)&=-B_{00}^{(0)}y^2/2-b_{00}^{(0)}x^2/2 \qquad (29)\\
&+(\varepsilon A_{11}^{(1)}(t))\left[-B_{00}^{(1)}y^2/2-b_{00}^{(1)}x^2/2+b_{111}\sin mx\sin ny\right]\\
&+\left(\varepsilon\frac{\partial^2 A_{11}^{(1)}(t)}{\partial t^2}\right)b_{311}\sin mx\sin ny\\
&+(\varepsilon A_{11}^{(1)}(t))^2\left[-B_{00}^{(2)}y^2/2-b_{00}^{(2)}x^2/2+b_{202}\cos\ 2ny\right.\\
&\left.+b_{220}\cos\ 2mx\right]\\
&+(\varepsilon A_{11}^{(1)}(t))^3[b_{331}\sin\ 3mx\sin\ ny\\
&+b_{313}\sin\ mx\sin\ 3ny]+O(\varepsilon^4)
\end{aligned}$$

$$\begin{aligned}
\lambda_q(x,y,t)&=\varepsilon\left[g_{31}A_{11}^{(1)}(t)+g_{30}\left(\frac{\partial^2 A_{11}^{(1)}(t)}{\partial t^2}\right)\right] \qquad (30)\\
&\cdot\sin mx\sin ny\\
&+(\varepsilon A_{11}^{(1)}(t))^2[g_{220}\cos\ 2mx+g_{202}\cos\ 2ny]\\
&+\left(\varepsilon A_{11}^{(1)}(t)\right)^3[g_{33}\sin mx\sin ny]+\ldots
\end{aligned}$$

It is worth noting that the perturbation series is a divergent series. Which order solution is closer to the real solution needs to be determined by experimental verification or by comparing with the theoretical exact solution. Contrary to Zhang's conclusion [63], there is no such thing as a

Table 1: Temperature-dependent material properties of monolayer graphene (a_G = 14.76 nm, b_G = 14.77 nm, thickness h_G = 0.188 nm, ν_{12}^G = 0.177, ρ_G = 4118 kg/m^3) [46].

Temperature (K)	E_{11}^G (GPa)	E_{22}^G (GPa)	G_{12}^G (GPa)	α_{11}^G (10^{-6}/K)	α_{22}^G (10^{-6}/K)
300	1812	1807	683	−0.90	−0.95
400	1769	1763	691	−0.35	−0.40
500	1748	1735	700	−0.08	−0.08

Table 2: Temperature dependent efficiency parameters of graphene/PMMA nanocomposites [36]

T (K)	V_G	η_1	η_2	η_3
300	0.03	2.929	2.855	11.842
	0.05	3.068	2.962	15.944
	0.07	3.013	2.966	23.575
	0.09	2.647	2.609	32.816
	0.11	2.311	2.260	33.125
400	0.03	2.977	2.896	13.928
	0.05	3.128	3.023	15.229
	0.07	3.060	3.027	22.588
	0.09	2.701	2.603	28.869
	0.11	2.405	2.337	29.527
500	0.03	3.388	3.382	16.712
	0.05	3.544	3.414	16.018
	0.07	3.462	3.339	23.428
	0.09	3.058	2.936	29.754
	0.11	2.736	2.665	30.773

higher order perturbation solution being more correct than a lower order solution.

In Eqs. (26)-(30), τ is replaced back by t. It is noted that the small perturbation parameter ε is replaced by $(\varepsilon A_{11}^{(1)})$ in the second step. For free vibration analysis, applying Galerkin procedure to Eq. (30), we have

$$g_{30}\frac{d^2(\varepsilon A_{11}^{(1)})}{dt^2} + g_{31}(\varepsilon A_{11}^{(1)}) + g_{32}(\varepsilon A_{11}^{(1)})^2 + g_{33}(\varepsilon A_{11}^{(1)})^3 = 0 \tag{31}$$

in which the terms g_{ij} are given in Appendix C. Eq. (31) can be solved to obtain the nonlinear frequency of the panel as follows

$$\omega_{NL} = \omega_L\left[1 + \frac{9g_{31}g_{33} - 10g_{32}^2}{12g_{31}^2}A^2\right]^{1/2} \tag{32}$$

where $\omega_L = [g_{31}/g_{30}]^{1/2}$ is the dimensionless linear frequency, and $A = W_{max} = \overline{W}_{\max}/[D_{11}^* D_{22}^* A_{11}^* A_{22}^*]^{1/4}$ is the dimensionless maximum amplitude of the panel. It is worth noting that Eqs. (31) and (32) are similar in form to those of the cylindrical panels [50], but have different contents, as shown in Appendix C.

4 Numerical results and discussion

In this section, numerical results for the nonlinear vibration of doubly curved GRC laminated panels resting on elastic foundations and under different thermal environmental conditions are obtained. It is noted that the material properties of graphene sheets are anisotropic [24–26] and temperature dependent [27]. We select zigzag (refer to as 0-ply) graphene sheets with effective thickness h_G = 0.188 nm and ρ_G = 4118 kg/m^3 as reinforcement agents. Lin *et al.* [46] performed a molecular dynamics simulation to evaluate the material properties of graphene sheets at different temperatures. These material properties at three different temperature levels are provided in Table 1. It must be pointed out that the Young's modulus of single-layer graphene sheet is not a constant which depends on the value of its effective thickness [64]. For example, it has been reported that Young's modulus of single-layer graphene sheet is estimated to be about 1 TPa. This is due to the fact that the effective thickness of graphene sheet is taken to be 0.34 nm [65, 66], otherwise the Young's modulus may reach 2.47 TPa which is significantly larger than that reported in [65, 66], when the effective thickness of graphene sheet is only 0.129 nm [27]. In the MD work of Lin *et al.* [46], the calculated effective thickness of the graphene sheet is 0.188 nm according to the research findings of Shen *et al.* [27]. Therefore, the predicted Young's moduli of the graphene sheet (see in Table 1) reach around 1.8 TPa. The graphene efficiency parameters η_1, η_2 and η_3 used in the extended Halpin-Tsai micromechanical model are given in Table 2 which are obtained by comparing the GRC moduli from the MD simulations and from the Halpin–Tsai model, as previously reported in Shen *et al.* [36]. We assume that $G_{13} = G_{23} = 0.5G_{12}$. We select Poly (methyl methacrylate), referred to as PMMA, for the matrix. The material properties of PMMA are assumed to be ρ^m = 1150 kg/m^3, ν^m = 0.34, α^m = 45(1+0.0005ΔT)×10^{-6}/K and E^m = (3.52-0.0034T) GPa, in which $T = T_0$ + and T_0 = 300 K (room temperature). Hence, we have α^m = 45.0×10^{-6}/K and E^m = 2.5 GPa when T = 300 K.

Comparison studies are carried to verify the correctness of the present solution method. The fundamental fre-

Table 3: Comparison of linear frequency $\tilde{\Omega} = \Omega(a^2/h)\sqrt{\rho_0/E_0}$ for double curved CNT/PmPV panels ($a/b = 1$, $a/h = 20$, $a/R_1 = b/R_2 = 0.5$, $T = 300$K)

V^*_{CN}	Source		UD	FG-Λ	FG-V	FG-X	FG-O
11	Pouresmaeeli Fazelzadeh [67]	&	20.2381	18.2514	18.5425	22.4320	17.1397
	Present		20.2587	18.8587	18.7062	24.0664	16.9807
14	Pouresmaeeli Fazelzadeh [67]	&	21.6551	19.5458	19.7789	23.9965	18.2670
	Present		21.7298	20.0403	19.9679	26.1019	18.1251
17	Pouresmaeeli Fazelzadeh [67]	&	25.0512	22.6250	22.9514	27.8527	21.2115
	Present		25.1226	22.9894	23.1790	29.8651	21.0842

quencies from the present method and from Pouresmaeeli and Fazelzadeh [67] using the Galerkin method for CNTRC doubly curved panels with $a/b = 1$, $a/h = 20$ and $a/R_1 = b/R_2 = 0.5$ are presented in Table 3. Note that Pouresmaeeli and Fazelzadeh [67] employed the first order shear deformation theory with the shear correction factor of 5/6 in their analysis. The dimensionless frequency is defined by $\tilde{\Omega} = \Omega(a^2/h)\sqrt{\rho_0/E_0}$, with ρ_0 and E_0 being the reference values of PmPV at room temperature $T = 300$ K. In Table 3, the extended Voigt model (rule of mixture) is adopted and the CNT efficiency parameters are taken to be $\eta_1 = 0.149$, $\eta_2 = \eta_3 = 0.934$ for the case of = 0.11, and $\eta_1 = 0.150$, $\eta_2 = \eta_3 = 0.941$ for the case of $V^*_{CN} = 0.14$, and $\eta_1 = 0.149$, $\eta_2 = \eta_3 = 1.381$ for the case of $V^*_{CN} = 0.17$. It can be seen that for the UD, FG-Λ, FG-V and FG-X cases the results of Pouresmaeeli and Fazelzadeh [67] are lower than the present solutions whereas for the FG-O case the results of Pouresmaeeli and Fazelzadeh [67] are higher than the present solutions. As a second example, the dimensionless fundamental frequencies for Al/ZrO_2 doubly curved panels, which have ceramic-rich outer surface and metal-rich inner surface, are calculated and compared in Table 4 with the analytical hybrid Laplace–Fourier transformation results of Kiani *et al.* [11] and the isoparametric finite element approach results of Kar and Panda [13]. The conventional Voigt model was adopted by Kiani *et al.* [11] and Kar and Panda [13]. The value of N in Table 4 is the index of volume fraction. The material properties of the panels do not include the effect of temperature with the properties of Aluminum being $E_m = 70$ GPa, $\nu_m = 0.3$ and $\rho_m = 2702$ kg/m^3 and Zirconia being $E_c = 151$ GPa, $\nu_c = 0.3$, and $\rho_c = 3000$ kg/m^3. The third comparison study is presented in Figure 2 on the nonlinear-to-linear frequency ratios ω_{NL}/ω_L for a (0/90/0) laminated square spherical panel from the present method and from the FEM results of Singh and Panda [4] based on a higher order shear deformation theory. The panel is of movable in-plane boundary condition. The geometric parameters and the material properties used in the computation study are: $a/b = 1$, $b/h = 100$, $R_1/a = 5$, $R_2/b = 5$, $E_{11} = 40E_{22}$, $G_{23} = 0.5E_{22}$, $G_{12} = G_{13} = 0.6E_{22}$, $\nu_{12} = 0.25$. Only the vibration mode of $(m, n) = (1, 1)$ is considered. The three comparison studies have shown that good agreement is achieved between the results from the present solution method and from existing research work in the open literature.

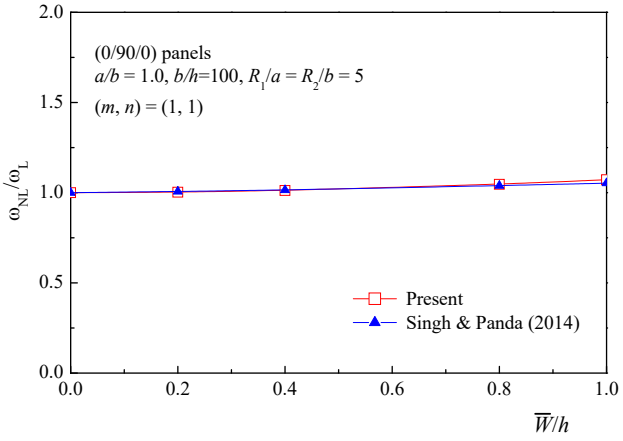

Figure 2: Comparisons of frequency-amplitude curves of a (0/90/0) laminated square spherical panel

Tables 5-7 and Figures 3-7 present the numerical results for the large amplitude vibration of doubly curved GRC laminated panels with $h = 2$ mm, $a/b = 1.0$, $b/h = 10$ and 20. Note that GRCs may contain the volume fraction of graphene reinforcement by up to 21% [68] and in this study the maximum graphene volume fraction is 11%. Four FG and one UD GRC laminated doubly curved panels are considered. The UD GRC panel consists of 10 GRC layers with the graphene volume fraction for each layer being identical, *i.e.* $V_G = 0.07$. The four FG-GRC panels consist of 10 GRC layers with piece-wise graphene volume fractions, *i.e.* the

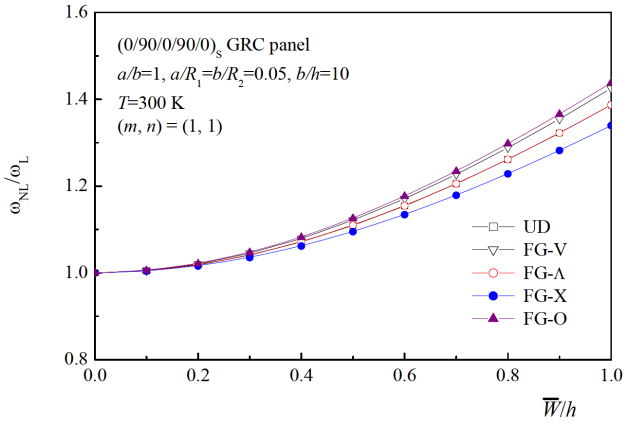

Figure 3: Frequency-amplitude curves for doubly curved $(0/90/0/90/0)_S$ GRC laminated panels with different graphene distribution patterns

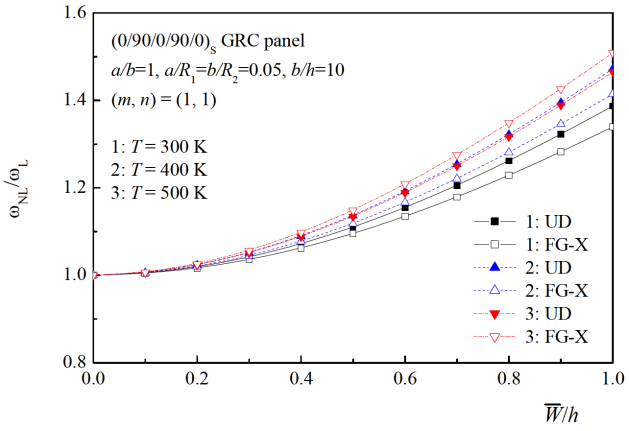

Figure 4: Influence of temperature variation on the frequency-amplitude curves of doubly curved $(0/90/0/90/0)_S$ GRC laminated panels

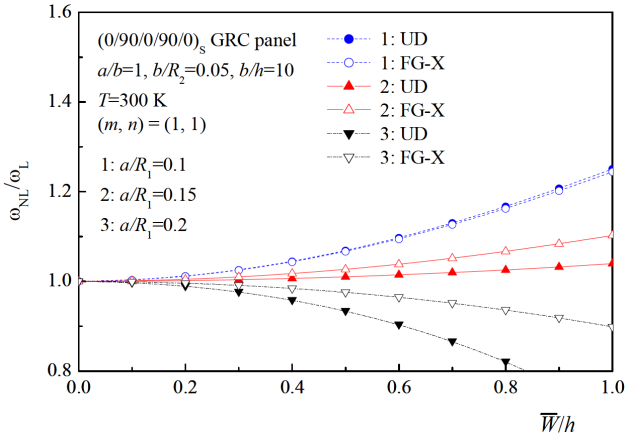

Figure 5: Influence of panel curvature ratio a/R_1 on the frequency-amplitude curves of doubly curved $(0/90/0/90/0)_S$ GRC laminated panels

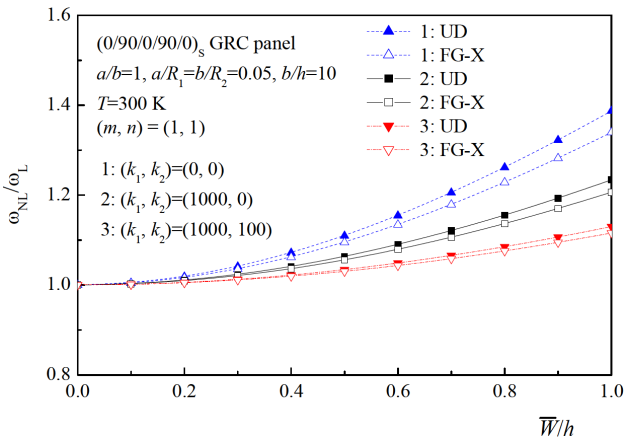

Figure 6: Influence of foundation stiffness on the frequency-amplitude curves of doubly curved $(0/90/0/90/0)_S$ GRC laminated panels resting on elastic foundations

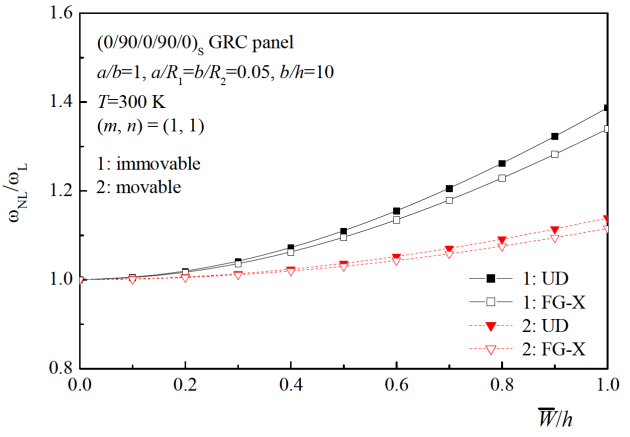

Figure 7: Influence of in-plane boundary conditions on the frequency-amplitude curves of doubly curved $(0/90/0/90/0)_S$ GRC laminated panels

FG-Λ type with $[(0.03)_2/(0.05)_2/(0.07)_2/(0.09)_2/(0.11)_2]$, the FG-V with $[(0.11)_2/(0.09)_2/(0.07)_2/(0.05)_2/(0.03)_2]$, the FG-O type with $[0.03/0.05/0.07/0.09/0.11]_S$ and the FG-X type with $[0.11/0.09/0.07/0.05/0.03]_S$. Note that the total graphene volume fraction for all considered GRC laminated panels are the same. The non-dimensional frequency parameter $\tilde{\Omega} = \Omega\left(b^2/h\right)\sqrt{\rho_0/E_0}$ is used in this study, where ρ_0 and E_0 are the reference values of ρ^m and E^m at $T = 300$ K. The panels are simply supported with immovable in-plane condition, unless stated otherwise.

Table 5 presents the natural frequencies of $(0)_{10}$, $(0/90/0/90/0)_S$ and $(0/90)_{5T}$ doubly curved GRC laminated panels having $b/h = 20$ and $a/R_1 = b/R_2 = 0.4$ with environmental temperature $T = 300$ and 400 K. It is observed that increasing the environmental temperature will result in the decrease in the natural frequencies of the panels

Table 4: Comparisons of fundamental frequencies $\tilde{\omega} = \Omega(b^2/h)\sqrt{\rho_c/E_c}$ for double curved Al/ZrO_2 panels ($a/b = 1$, $b/h = 10$, $R_1 = 2R_2$)

R_2/b	$\tilde{\Omega}$	N					
		0	0.5	1.0	2.0	5.0	10.0
3	Kiani *et al.* [11]	6.2330	5.6206	5.3523	5.1435	4.9642	4.8300
	Kar and Panda [13]	6.2277	5.6191	5.3501	5.1377	4.9540	4.8214
	Present[a]	6.2806	5.6761	5.4091	5.1976	5.0096	4.8711
	Present[b]	6.2806	5.5405	5.2983	5.1156	4.9376	4.8078
5	Kiani *et al.* [11]	5.9412	5.3492	5.0960	4.9077	4.7515	4.6244
	Kar and Panda [13]	5.9394	5.3505	5.0963	4.9039	4.7428	4.6174
	Present[a]	5.9585	5.3732	5.1211	4.9302	4.7668	4.6380
	Present[b]	5.9585	5.2455	5.0205	4.8577	4.6999	4.5768
10	Kiani *et al.* [11]	5.8128	5.2310	4.9851	4.8062	4.6599	4.5354
	Kar and Panda [13]	5.8127	5.2333	4.986	4.8028	4.6515	4.5288
	Present[a]	5.8173	5.2403	4.9946	4.8129	4.6607	4.5360
	Present[b]	5.8173	5.1157	4.8985	4.7448	4.5961	4.4759
20	Kiani *et al.* [11]	5.7802	5.2018	4.9580	4.7816	4.6376	4.5135
	Kar and Panda [13]	5.7805	5.2041	4.9589	4.7782	4.6291	4.5068
	Present[a]	5.7815	5.2065	4.9625	4.7831	4.6337	4.5102
	Present[b]	5.7815	5.0826	4.8675	4.7163	4.5700	4.4505
100	Kiani *et al.* [11]	5.7698	5.1932	4.9504	4.7749	4.6315	4.5071
	Kar and Panda [13]	5.7701	5.1954	4.951	4.7712	4.6227	4.5003
	Present[a]	5.7699	5.1956	4.9522	4.7736	4.6251	4.5019
	Present[b]	5.7699	5.0718	4.8575	4.7073	4.5617	4.4424

[a] Voigt model; [b] Mori-Tanaka model.

due to the stiffness of the panels being reduced at a higher temperature. Results in Table 5 also reveal that the panel with the FG-X reinforcement pattern has the largest, while the panel with the FG-O pattern has the smallest natural frequencies in the five considered cases. Like in the case of cylindrical panels [50], the doubly curved GRC panels with $(0/90/0/90/0)_S$ and $(0/90)_{5T}$ lamination arrangements have the same fundamental frequencies which are slight higher than the ones for the panels with $(0)_{10}$ lamination arrangement at $T = 300$ K.

Table 6 presents the effect of foundation stiffness on the natural frequencies of $(0/90/0/90/0)_S$ doubly curved GRC laminated panels with $b/h = 20$, $b/R_2 = 0.4$ and $a/R_1 = 0.2$ and 0.8 under thermal environmental condition $T = 300$ K. We consider two foundation models which are the Pasternak elastic foundation with $(k_1, k_2) = (1000, 100)$ and the Winkler elastic foundation with $(k_1, k_2) = (1000, 0)$. The panel without elastic foundation, *i.e.* $(k_1, k_2) = (0, 0)$, is also considered. Like in the case of cylindrical panels [50], the natural frequency is increased when the foundation stiffness is increased at room temperature.

The impact of the in-plane boundary conditions on the nonlinear vibration behavior of the $(0/90/0/90/0)_S$ doubly curved GRC laminated panels is investigated and the results are presented in Table 7. The panels have the geometric parameters of $b/h = 10$ and $a/R_1 = b/R_2 = 0.02$ and are subject to environmental temperature of $T = 300$ and 400 K. The results in Table 7 show that when the panels are subject to room temperature, the fundamental frequencies for the panels with either the movable or the immovable in-plane boundary conditions are the same which is due to the fact that no initial in-plane thermal stresses are present in the panels in this case. However, when the panels are subject to temperature of $T = 400$ K, in-plane compressive thermal stresses are introduced to the panels with immovable in-plane boundary condition. Like in the case of cylindrical panels [50], the nonlinear-to-linear frequency ratios for the panel with movable in-plane boundary condition are smaller than the one for the panel with immovable in-plane boundary condition.

Figure 3 depicts the frequency-amplitude curves for four FG and one UD doubly curved GRC laminated panels of $b/h = 10$ and $a/R_1 = b/R_2 = 0.05$ at room temperature of $T = 300$ K. The laminated arrangement of the panels is $(0/90/0/90/0)_S$. It is observed that amongst the five GRC panels, the FG-X panel has the highest fundamental frequency as it has the largest panel stiffness, while the FG-O GRC panel has the lowest fundamental frequency as it has

Table 5: Natural frequency $\tilde{\Omega} = \Omega(b^2/h)\sqrt{\rho_0/E_0}$ of double curved GRC laminated panels in thermal environments ($a/b = 1$, $b/h = 20$, $h = 2$ mm, $a/R_1 = b/R_2 = 0.4$)

T (K)	Lay-up		(1,1)[a]	(1,2)	(2,1)	(2,2)	(1,3)
300	$(0)_{10}$	UD	48.3014	82.6496	82.8618	118.5889	146.2361
		FG-V	45.0530	74.4394	74.7672	106.6529	131.3309
		FG-Λ	47.0308	76.4596	76.7165	109.7334	132.7072
		FG-X	49.2661	85.4987	85.7574	123.8480	149.7251
		FG-O	44.8643	71.4763	71.7414	101.4378	124.5773
	$(0/90/0/90/0)_S$	UD	48.3017	82.7196	82.7923	118.5891	146.4664
		FG-V	45.0534	74.5451	74.6625	106.6531	131.6821
		FG-	47.0316	76.5387	76.6388	109.7343	133.0248
		FG-X	49.2667	85.5555	85.7016	123.8484	149.9319
		FG-O	44.8650	71.6196	71.5993	101.4382	125.0769
	$(0/90)_{5T}$	UD	48.3017	82.7651	82.7467	118.5890	146.5894
		FG-V	45.0534	74.6258	74.5817	106.6530	131.8956
		FG-Λ	47.0316	76.5930	76.5844	109.7342	133.1821
		FG-X	49.2666	85.6444	85.6125	123.8482	150.1496
		FG-O	44.8650	71.6066	71.6122	101.4382	125.0617
400	$(0)_{10}$	UD	34.2138	57.5011	67.5649	94.5042	114.5018
		FG-V	36.1359	50.9012	61.1003	85.2160	101.3850
		FG-Λ	30.5796	51.8494	62.2123	86.4531	102.7173
		FG-X	36.2822	63.0136	71.6413	101.1963	120.8419
		FG-O	31.2439	45.8868	56.8932	78.1132	92.6827
	$(0/90/0/90/0)_S$	UD	34.2140	61.7114	63.7426	94.5043	120.2617
		FG-V	36.1360	55.0395	57.4023	85.2169	107.2002
		FG-Λ	30.5811	56.0494	58.4583	86.4537	108.6451
		FG-X	36.2833	66.6612	68.2621	101.1972	126.1756
		FG-O	31.2451	50.7250	52.6267	78.1138	99.4918
	$(0/90)_{5T}$	UD	34.2139	62.7425	62.7280	94.5043	121.7073
		FG-V	36.1360	56.2466	56.2198	85.2167	108.9418
		FG-Λ	30.5810	57.2915	57.2412	86.4534	110.4587
		FG-X	36.2833	67.4694	67.4635	101.1972	127.3658
		FG-O	31.2450	51.668	51.7008	78.1137	100.7452

[a] vibration mode

the smallest panel stiffness. It is also observed that the FG-X panel has the lowest and the FG-O has the highest nonlinear to linear frequency ratios in the considered cases. We will focus our analysis on the doubly curved UD and FG-X GRC $(0/90/0/90/0)_S$ panels for the subsequent cases.

Figure 4 shows the effect of temperature variation on the large amplitude vibration behavior of doubly curved UD and FG-X laminated panels with $b/h = 10$ and $a/R_1 = b/R_2 = 0.05$. Note that the glass transition temperature of PMMA can be substantially increased when graphene sheets are added in PMMA [69] and in the current study, we will consider the environmental temperature variation from $T = 300$ to 500K. It can be seen that for the cases of $T = 300$ and 400K, the frequency-amplitude curve increases with increase in temperature for both UD and FG-X GRC panels, whereas for the case of $T = 500$ K, the frequency-amplitude curve of the FG-X GRC panel becomes higher than that of the UD GRC panel.

The influence of the curvature ratio a/R_1 on the frequency-amplitude curves of the doubly curved UD and FG-X panels of $b/h = 10$, $b/R_2 = 0.05$ and $a/R_1 = 0.1$, 0.15 and 0.2 at room temperature of $T = 300$ K is given in Figure 5. As previously reported in [1–3], the curves of nonlinear frequency as a function of amplitude of curved panels might be hardening or softening type. It is observed that the nonlinear frequency as a function of amplitude of the GRC laminated doubly curved panel is the softening type when $a/R_1 = 0.2$. For other cases, the nonlinear frequency

Table 6: Effects of foundation stiffness on the natural frequency $\tilde{\Omega} = \Omega(b^2/h)\sqrt{\rho_0/E_0}$ of double curved $(0/90/0/90/0)_S$ GRC laminated panels. ($a/b = 1$, $b/h = 20$, $h = 2$ mm, $b/R_2 = 0.4$, $T = 300$K)

(k_1, k_2)	a/R_1		(1,1)[a]	(1,2)	(2,1)	(2,2)	(1,3)
(0, 0)	0.2	UD	41.1721	76.5493	81.0143	115.8924	142.6105
		FG-V	37.8351	68.4411	72.8904	104.1301	128.0025
		FG-Λ	39.5992	69.7487	74.7134	106.5038	128.7642
		FG-X	42.4981	79.9146	84.0718	121.3349	146.4308
		FG-O	37.3048	64.7792	69.6411	98.3588	120.8690
	0.8	UD	64.4642	101.4007	86.7702	125.9762	160.0728
		FG-V	61.3089	93.2844	78.6432	113.8672	145.1027
		FG-Λ	63.4989	96.1479	80.8929	118.1785	147.4119
		FG-X	64.8215	102.8914	89.3618	130.7637	162.3642
		FG-O	61.5448	91.6238	75.9404	109.7616	139.7027
(1000, 0)	0.2	UD	50.3874	81.8504	86.0407	119.4462	145.5074
		FG-V	47.6990	74.3210	78.4375	108.0687	131.2189
		FG-Λ	49.1102	75.5272	80.1347	110.3581	131.9623
		FG-X	51.4760	85.0073	88.9267	124.7367	149.2571
		FG-O	47.2807	70.9640	75.4283	102.5191	124.2693
	0.8	UD	70.7063	105.4599	91.4809	129.2531	162.6590
		FG-V	67.8414	97.6801	83.8104	117.4797	147.9477
		FG-	69.8272	100.4187	85.9253	121.6637	150.2136
		FG-X	71.0318	106.8950	93.9437	133.9262	164.9176
		FG-O	68.0557	96.0961	81.2803	113.5048	142.6548
(1000, 100)	0.2	UD	64.8411	104.1308	107.4558	144.4679	171.4938
		FG-V	62.7740	98.3161	101.4637	135.1959	159.5227
		FG-Λ	63.8533	99.2318	102.7823	137.0349	160.1359
		FG-X	65.6898	106.6346	109.7848	148.8911	174.7155
		FG-O	62.4587	95.8065	99.1586	130.8007	153.8491
	0.8	UD	81.6386	123.5538	111.8593	152.6759	186.2677
		FG-V	79.1696	116.9774	105.6720	142.8296	173.5434
		FG-Λ	80.8782	119.2755	107.3585	146.2942	175.4819
		FG-X	81.9200	124.7848	113.8866	156.6703	188.2702
		FG-O	79.3549	115.6610	103.6798	139.5779	169.0476

[a] vibration mode

as a function of amplitude of the GRC laminated doubly curved panels is the hardening type.

The impact of foundation stiffness on the frequency-amplitude curves of UD and FG-X doubly curved panels resting on elastic foundations is illustrated in Figure 6. The panel has $b/h = 10$ and $a/R_1 = b/R_2 = 0.05$ at $T = 300$ K. Two foundation models are considered. The foundation stiffnesses are the same as used in Table 6, *i.e.*, $(k_1, k_2) = (1000, 100)$ is for the Pasternak elastic foundation, and $(k_1, k_2) = (1000, 0)$ is for the Winkler elastic foundation. As expected, increasing the foundation stiffness will result in the reduction of the frequency-amplitude curves of the panels.

Figure 7 presents the relationship between the in-plane boundary conditions and the frequency-amplitude curves of the doubly curved UD and FG-X panels with $b/h = 10$ and $a/R_1 = b/R_2 = 0.05$ at $T = 300$ K. The 'movable' and 'immovable' in-plane boundary conditions are considered. It is observed that the nonlinear-to-linear frequency ratios for panels with immovable in-plane boundary conditions are larger than the ones for the panels with movable in-plane boundary conditions.

Table 7: Effects of end condition on the nonlinear to linear frequency ratios ω_{NL}/ω_L for double curved $(0/90/0/90/0)_S$ GRC laminated panels in thermal environments ($a/b = 1$, $b/h = 10$, $h = 2$ mm, $a/R_1 = b/R_2 = 0.02$)

T (K)		$\tilde{\Omega}$	$\overline{W}_{\max}/h$				
			0.2	0.4	0.6	0.8	1.0
in-plane immovable boundary condition							
300	UD	28.0986	1.0232	1.0898	1.1926	1.3232	1.4742
	FG-V	25.3511	1.0258	1.0997	1.2129	1.3556	1.5195
	FG-Λ	25.4331	1.0249	1.0963	1.2059	1.3444	1.5039
	FG-X	29.5211	1.0191	1.0744	1.1607	1.2717	1.4016
	FG-O	23.5816	1.0292	1.1122	1.2382	1.3957	1.5752
400	UD	21.9646	1.0333	1.1274	1.2688	1.4437	1.6414
	FG-V	19.6591	1.0364	1.1386	1.2910	1.4782	1.6887
	FG-	19.6816	1.0388	1.1475	1.3087	1.5056	1.7262
	FG-X	23.8171	1.0260	1.1003	1.2141	1.3575	1.5222
	FG-O	17.5688	1.0455	1.1714	1.3555	1.5775	1.8237
in-plane movable boundary condition							
300	UD	28.0986	1.0061	1.0242	1.0537	1.0936	1.1429
	FG-V	25.3511	1.0068	1.0269	1.0596	1.1037	1.1580
	FG-Λ	25.4331	1.0066	1.0262	1.0580	1.1011	1.1540
	FG-X	29.5211	1.0050	1.0199	1.0442	1.0773	1.1184
	FG-O	23.5816	1.0078	1.0308	1.0681	1.1183	1.1796
400	UD	26.2383	1.0063	1.0249	1.0552	1.0963	1.1469
	FG-V	23.8420	1.0068	1.0271	1.0600	1.1044	1.1590
	FG-Λ	24.0202	1.0070	1.0278	1.0616	1.1071	1.1631
	FG-X	27.3880	1.0052	1.0208	1.0462	1.0807	1.1235
	FG-O	22.1643	1.0080	1.0314	1.0695	1.1205	1.1829

5 Concluding remarks

Applying a multi-scale approach, a large amplitude vibration analysis of doubly curved GRC laminated panels has been carried out. The panels are supported by an elastic foundation and in thermal environments. The piecewise functionally graded (FG) GRC layer arrangement is considered to achieve the UD, FG-X, FG-O, FG-V and FG-Λ laminated panels in this study. The extended Halpin-Tsai model is employed to evaluate the material properties of GRC layers which includes the thermal effect on both the graphene sheets and the polymer matrix. Results for large amplitude vibration of doubly curved UD and FG GRC laminated panels are obtained and discussed in detail. Like in the case of cylindrical panels, the rise of temperature will lead to the decrease of the natural frequencies and the increase of the nonlinear-to-linear frequency ratios for the doubly curved GRC laminated panels. On the other hand, the increase of foundation stiffness will result in the increase of the natural frequencies and the decrease of the nonlinear-to-linear frequency ratios of the panels. We observed that the FG-X panel has the highest fundamental frequency but the lowest nonlinear-to-linear frequency ratios and the FG-O panel has the lowest fundamental frequency but the highest nonlinear-to-linear frequency ratios in the considered cases. Unlike in the case of cylindrical panels where both UD and FG-GRC panels display a hardening nonlinearity, in some cases the frequency-amplitude curves of the doubly curved UD and FG-GRC laminated panels exhibit a softening nonlinear behavior at room temperature.

Acknowledgement: This study was supported by the National Natural Science Foundation of China under Grant 51779138 and the Australian Research Council under Grant DP140104156. The authors are very grateful for these financial supports.

Conflict of Interests: The authors declare that there are no conflicts of interests with publication of this work.

References

[1] Cummings B.E., Large-amplitude vibration and response of curved panels, AIAA J., 1964, 2, 709-716.

[2] Shin D.K., Large amplitude free vibration behavior of doubly curved shallow open shells with simply-supported edges, Comput. Struct., 1997, 62, 35-49.

[3] Panda S.K., Singh B.N., Nonlinear free vibration of spherical shell panel using higher order shear deformation theory - A finite element approach, Int. J. Pres. Vess. Pip., 2009, 86, 373-383.

[4] Singh V.K., Panda S.K., Nonlinear free vibration analysis of single/doubly curved composite shallow shell panels, Thin-Walled Struct., 2014, 85, 341-349.

[5] Mahapatra T.R., Panda S.K., Thermoelastic vibration analysis of laminated doubly curved shallow panels using non-linear FEM, J. Thermal Stress., 2015, 38, 39-68.

[6] Karimiasl M., Ebrahimi F., Vinyas M., Nonlinear vibration analysis of multiscale doubly curved piezoelectric composite shell in hygrothermal environment, J. Intelligent Mater. Systems Struct., 2019, 30, 1594-1609.

[7] Karimiasl M., Ebrahimi F., Mahesh V., Nonlinear free and forced vibration analysis of multiscale composite doubly curved shell embedded in shape-memory alloy fiber under hygrothermal environment, J. Vib. Control, 2019, 25, 1945-1957.

[8] Karimiasl M., Ebrahimi F., Mahesh V., Nonlinear forced vibration of smart multiscale sandwich composite doubly curved porous shell, Thin-Walled Struct., 2019, 143, 106152.

[9] Shen H.-S., Functionally Graded Materials Nonlinear Analysis of Plates and Shells, CRC Press, Boca Raton, 2009.

[10] Shen H.-S., Nonlinear bending of functionally graded carbon nanotube-reinforced composite plates in thermal environments, Compos. Struct., 2009, 91, 9-19.

[11] Kiani Y., Shakeri M., Eslami M.R., Thermoelastic free vibration and dynamic behaviour of an FGM doubly curved panel via the analytical hybrid Laplace-Fourier transformation, Acta Mech., 2012, 223, 1199-1218.

[12] Shen H.-S., Chen X., Guo L., Wu L., Huang X.-L., Nonlinear vibration of FGM doubly curved panels resting on elastic foundations in thermal environments, Aerospace Sci. Technol., 2015, 47, 434-446.

[13] Kar V.R., Panda S.K., Large-amplitude vibration of functionally graded doubly-curved panels under heat conduction, AIAA J., 2017, 55, 4376-4386.

[14] Fares M.E., Elmarghany M.K., Atta D., Salem M.G., Bending and free vibration of multilayered functionally graded doubly curved shells by an improved layerwise theory, Compos. Part B-Eng., 2018, 154, 272-284.

[15] Dong D.T., Dung D.V., A third-order shear deformation theory for nonlinear vibration analysis of stiffened functionally graded material sandwich doubly curved shallow shells with four material models, J. Sand. Struct. Mater., 2019, 21, 1316-1356.

[16] Talebitooti R., Anbardan V.S., Haar wavelet discretization approach for frequency analysis of the functionally graded generally doubly-curved shells of revolution, Appl. Math. Modell., 2019, 67, 645-675.

[17] Amir M., Talha M., Nonlinear vibration characteristics of shear deformable functionally graded curved panels with porosity including temperature effects, Int. J. Pres. Vess. Pip., 2019, 172, 28-41.

[18] Shen, H.-S., He, X.-Q.: Large amplitude free vibration of nanotube-reinforced composite doubly curved panels resting on elastic foundations in thermal environments. J. Vib. Control, 2017, 23, 2672-2689

[19] Duc N.D., Quan T.Q., Khoa N.D., New approach to investigate nonlinear dynamic response and vibration of imperfect functionally graded carbon nanotube reinforced composite double curved shallow shells subjected to blast load and temperature, Aerospace Sci. Technol., 2017, 71, 360-372.

[20] Mehar K., Panda S.K., Thermal free vibration behavior of FG-CNT reinforced sandwich curved panel using finite element method, Poly. Compos., 2018, 39, 2751-2764.

[21] Mehar K., Panda S.K., Mahapatra T.R., Nonlinear frequency responses of functionally graded carbon nanotube-reinforced sandwich curved panel under uniform temperature field, Int. J. Appl. Mech., 2018, 10, 1850028.

[22] Setoodeh A.R., Shojaee M., Malekzadeh P., Vibrational behavior of doubly curved smart sandwich shells with FG-CNTRC face sheets and FG porous core, Compos. Part B-Eng., 2019, 165, 798-822.

[23] Novoselov K.S., Geim A.K., Morozov S.V., Jiang D., Zhang Y., Dubonos S.V., Grigorieva I.V., Firsov A., Electric filed effect in atomically thin carbon films, Science, 2004, 306, 666-669.

[24] Liu F., Ming P.M., Li J., Ab initio calculation of ideal strength and phonon instability of graphene under tension, Phys. Rev. B, 2007, 76, 064120.

[25] Ni Z., Bu H., Zou M., Yi H., Bi K., Chen Y., Anisotropic mechanical properties of graphene sheets from molecular dynamics, Physica B, 2010, 405, 1301-1306.

[26] Reddy C.D., Rajendran S., Liew K.M., Equilibrium configuration and elastic properties of finite graphene, Nanotechnol., 2006, 17, 864-870.

[27] Shen L., Shen H.-S., Zhang C.-L., Temperature-dependent elastic properties of single layer graphene sheets, Mater. Des., 2010, 31, 4445-4449.

[28] Xu Z., Graphene nano-ribbons under tension, J. Comput. Theor. Nanosci., 2009, 6, 625-628.

[29] Potts J.R., Dreyer D.R., Bielawski C.W., Ruoff R.S., Graphene-based polymer nanocomposites, Polymer, 2011, 52, 5-25.

[30] Wang A., Chen H., Hao Y., Zhang W., Vibration and bending behavior of functionally graded nanocomposite doubly-curved shallow shells reinforced by graphene nanoplatelets, Results Phys., 2018, 9, 550-559.

[31] Wang A., Chen H., Zhang W., Nonlinear transient response of doubly curved shallow shells reinforced with graphene nanoplatelets subjected to blast loads considering thermal effects, Compos. Struct., 2019, 225, 111063.

[32] Fazelzadeh S.A., Rahmani S., Ghavanloo E., Marzocca P., Thermoelastic vibration of doubly-curved nano-composite shells reinforced by graphene nanoplatelets, J. Thermal Stress., 2019, 42, 1-17.

[33] Zhao X., Zhang Q., Hao Y., Li Y., Fang Y., Chen D., Alternate multilayer films of poly(vinyl alcohol) and exfoliated graphene oxide fabricated via a facial Layer-by-Layer assembly, Macromolecules, 2010, 43, 9411-9416.

[34] Liang Q., Yao X., Wang W., Liu Y., Wong C.P., A three-dimensional vertically aligned functionalized multilayer graphene architecture: an approach for graphene-based thermal interfacial materials, ACS Nano, 2011, 5, 2392-2401.

[35] Yousefi N., Sun X., Lin X., Shen X., Jia J., Zhang B., Tang B., Chan M., Kim J.-K., Highly aligned graphene/polymer nanocomposites with excellent dielectric properties for high-performance electromagnetic interference shielding, Adv. Mater., 2014, 26, 5480-5487.
[36] Shen H.-S., Xiang Y., Lin F., Nonlinear vibration of functionally graded graphene-reinforced composite laminated plates in thermal environments, Comput. Methods Appl. Mech. Eng., 2017, 319, 175-193.
[37] Lei Z., Su Q., Zeng H., Zhang Y., Yu C., Parametric studies on buckling behavior of functionally graded graphene-reinforced composites laminated plates in thermal environment, Compos. Struct. 2018, 202, 695-709.
[38] Kiani Y., Isogeometric large amplitude free vibration of graphene reinforced laminated plates in thermal environment using NURBS formulation, Comput. Methods Appl. Mech. Eng., 2018, 332, 86-101.
[39] Kiani Y., NURBS-based isogeometric thermal postbuckling analysis of temperature dependent graphene reinforced composite laminated plates, Thin-Walled Struct., 2018, 125, 211-219.
[40] Rout M., Hota S.S., Karrnakar A., Thermoelastic free vibration response of graphene reinforced laminated composite shells, Eng. Struct., 2019, 178, 179-190.
[41] Wang M., Xu Y.-G., Qiao P., Li Z.M., A two-dimensional elasticity model for bending and free vibration analysis of laminated graphene-reinforced composite beams, Compos. Struct., 2019, 211, 364-375.
[42] Lei Z.X., Tong L.H., Analytical solution of low-velocity impact of graphene-reinforced composite functionally graded cylindrical shells, J. Brazilian Society Mech. Sci. Eng., 2019, 41, 486.
[43] Ly L.N., Phuong N.T., Nam V.H., Trung N.T., Duc V.M., An analytical approach of nonlinear thermo-mechanical buckling of functionally graded graphene-reinforced composite laminated cylindrical shells under compressive axial load surrounded by elastic foundation, J. Appl. Comput. Mech., 2020, 6, 357-372.
[44] Halpin J.C., Kardos J.L., The Halpin-Tsai equations: A review, Polym. Eng. Sci., 1976, 16, 344-352.
[45] Hu K., Kulkarni D.D., Choi I., Tsukruk V.V., Graphene-polymer nanocomposites for structural and functional applications, Progress Polym. Sci., 2014, 39, 1934-1972.
[46] Lin F., Xiang Y., Shen H.-S., Temperature dependent mechanical properties of graphene reinforced polymer nanocomposites - a molecular dynamics simulation, Compos. Part B-Eng., 2017, 111, 261-269.
[47] Schapery R.A., Thermal expansion coefficients of composite materials based on energy principles, J. Compos. Mater., 1968, 2, 380-404.
[48] Reddy J.N., Liu C.F., A higher-order shear deformation theory of laminated elastic shells, Int. J. Eng. Sci., 1985, 23, 319-330.
[49] Shen H.-S., A Two-Step Perturbation Method in Nonlinear Analysis of Beams, Plates and Shells, John Wiley & Sons Inc., 2013.
[50] Shen H.-S., Xiang Y., Fan Y., Hui D., Nonlinear vibration of functionally graded graphene-reinforced composite laminated cylindrical panels resting on elastic foundations in thermal environments, Compos. Part B-Eng., 2018, 136, 177-186.
[51] Fu Y., Zhong J., Shao X., Chen Y., Thermal postbuckling analysis of functionally graded tubes based on a refined beam model, Int. J. Mech. Sci., 2015, 96-97, 58-64.
[52] Fu Y., Zhong J., Shao X., Tao C., Analysis of nonlinear dynamic stability for carbon nanotube-reinforced composite plates resting on elastic foundations, Mech. Adv. Mater. Struct., 2016, 23, 1284-1289.
[53] Zhong J., Fu Y., Wan D., Li Y., Nonlinear bending and vibration of functionally graded tubes resting on elastic foundations in thermal environment based on a refined beam model, Appl. Math. Modell., 2016, 40, 7601-7614.
[54] Fallah F., Nosier A., Sharifi M., Ghezelbash F., On perturbation method in mechanical, thermal and thermo-mechanical loadings of plates: cylindrical bending of FG plates, ZAMM, 2016, 96, 217-232.
[55] Najafi F., Shojaeefard M.H., Googarchin H.S., Nonlinear low-velocity impact response of functionally graded plate with nonlinear three-parameter elastic foundation in thermal field, Compos. Part B-Eng., 2016, 107, 123-140.
[56] Sahmani S., Aghdam M.M., Nonlocal strain gradient beam model for nonlinear vibration of prebuckled and postbuckled multilayer functionally graded GPLRC nanobeams, Compos. Struct., 2017, 179, 77-88.
[57] Babaei H., Kiani Y., Eslami M.R., Application of two-steps perturbation technique to geometrically nonlinear analysis of long FGM cylindrical panels on elastic foundation under thermal load, J. Thermal Stress., 2018, 41, 847-865.
[58] Babaei H., Kiani Y., Eslami M.R., Thermally induced large deflection analysis of shear deformable FGM shallow curved tubes using perturbation method, ZAMM, 2019, 99, 201800148.
[59] Babaei H., Kiani Y., Eslami M.R., Thermomechanical nonlinear in-plane analysis of fix-ended FGM shallow arches on nonlinear elastic foundation using two-step perturbation technique, Int. J. Mech. Mater. Des., 2019, 15, 225-244.
[60] Gao Y., Xiao W.-S., Zhu H., Free vibration analysis of nano-tubes consisted of functionally graded bi-semi-tubes by a two-steps perturbation method, Latin American J. Solids Struct., 2019, 16, 146.
[61] Gao Y., Xiao W.-S., Zhu H., Nonlinear vibration analysis of different types of functionally graded beams using nonlocal strain gradient theory and a two-step perturbation method, Euro. Phys. J. Plus, 2019, 134, 23.
[62] Shen H.-S., Nonlinear thermal bending of FGM cylindrical panels resting on elastic foundations under heat conduction, Compos. Struct., 2014, 113, 216-224.
[63] Zhang D., High-order analytical solutions and convergence discussions of the 2-step perturbation method for Euler-Bernoulli beams (in Chinese), Appl. Math. Mech., 2019, 40, 620-629.
[64] Shi J.-X., Natsuki T., Lei X.-W., Ni Q.-Q., Equivalent Young's modulus and thickness of graphene sheets for the continuum mechanical models, Appl. Phys. Lett., 2014, 104, 223101.
[65] Lee C., Wei X., Kysar J.W., Hone J., Measurement of the elastic properties and intrinsic strength of monolayer graphene, Science, 2008, 321, 385-388.
[66] Koenig S.P., Boddeti N.G., Dunn M.L., Bunch J.S., Ultrastrong adhesion of graphene membranes, Nat. Nanotechnol., 2010, 6, 543-546.
[67] Pouresmaeeli S., Fazelzadeh S.A., Frequency analysis of doubly curved functionally graded carbon nanotube-reinforced composite panels, Acta Mech., 2016, 227, 2765-2794.
[68] Putz K.W., Compton O.C., Palmeri M.J., Nguyen S.T., Brinson L.C., High-nanofiller-content graphene oxide-polymer nanocomposites via vacuum-assisted self-assembly, Adv. Funct. Mater., 2010, 20, 3322-3329.

[69] Ramanathan T., Abdala A.A., Stankovich S., Dikin D.A., Herrera-Alonso M., Piner R.D., Adamson D.H., Schniepp H.C., Chen X., Ruoff R.S., Nguyen S.T., Aksay I.A., Prud'Homme R.K., Brinson L.C., Functionalized graphene sheets for polymer nanocomposites, Nature Nanotechnol., 2008, 3, 327-331.

[70] Shen H.-S., Kármán-type equations for a higher-order shear deformation plate theory and its use in the thermal postbuckling analysis, Appl. Math. Mech., 1997, 18, 1137-1152.

Appendix A

In Eqs. (5)-(8), the thermal forces, moments and higher order moments $\overline{N}^T$, $\overline{M}^T$ and $\overline{P}^T$ of the shell are evaluated by

$$\begin{bmatrix} \overline{N}_x^T & \overline{M}_x^T & \overline{P}_x^T \\ \overline{N}_y^T & \overline{M}_y^T & \overline{P}_y^T \\ \overline{N}_{xy}^T & \overline{M}_{xy}^T & \overline{P}_{xy}^T \end{bmatrix} = \sum_{k=1}^{N} \int_{h_{k-1}}^{h_k} \begin{bmatrix} A_x \\ A_y \\ A_{xy} \end{bmatrix}_k (1, Z, Z^3) \Delta T \, dZ \tag{A.1a}$$

and $\overline{S}^T$ are defined by

$$\begin{bmatrix} \overline{S}_x^T \\ \overline{S}_y^T \\ \overline{S}_{xy}^T \end{bmatrix} = \begin{bmatrix} \overline{M}_x^T \\ \overline{M}_y^T \\ \overline{M}_{xy}^T \end{bmatrix} - \frac{4}{3h^2} \begin{bmatrix} \overline{P}_x^T \\ \overline{P}_y^T \\ \overline{P}_{xy}^T \end{bmatrix} \tag{A.1b}$$

in which $\Delta T = T - T_0$ is the change of temperature with respect to a predefined reference temperature T_0 at which the panel does no subject to any thermal strains, and

$$\begin{bmatrix} A_x \\ A_y \\ A_{xy} \end{bmatrix} = - \begin{bmatrix} \overline{Q}_{11} & \overline{Q}_{12} & \overline{Q}_{16} \\ \overline{Q}_{12} & \overline{Q}_{22} & \overline{Q}_{26} \\ \overline{Q}_{16} & \overline{Q}_{26} & \overline{Q}_{66} \end{bmatrix} \begin{bmatrix} 1 & 0 \\ 0 & 1 \\ 0 & 0 \end{bmatrix} \begin{bmatrix} \alpha_{11} \\ \alpha_{22} \end{bmatrix} \tag{A.2}$$

in which α_{11} and are the thermal expansion coefficients for the kth ply, $\overline{Q}_{ij}$ are the transformed elastic constants for a GRC layer. Note that $\overline{Q}_{ij} = Q_{ij}$ as zigzag or armchair graphene sheet is used in the GRC layer and

$$\begin{aligned} &Q_{11} = \frac{E_{11}}{1 - \nu_{12}\nu_{21}}, \quad Q_{22} = \frac{E_{22}}{1 - \nu_{12}\nu_{21}}, \\ &Q_{12} = \frac{\nu_{21} E_{11}}{1 - \nu_{12}\nu_{21}}, \\ &Q_{16} = Q_{26} = 0, \quad Q_{66} = G_{12}, Q_{44} = G_{23}, \quad Q_{55} = G_{13} \end{aligned} \tag{A.3}$$

where E_{11}, E_{22}, G_{12}, are the effective Young's and shear moduli and ν_{12} and ν_{21} are the Poisson's ratios of the GRC layer, respectively.

The inertias $I_i (i = 1, 2, 3, 4, 5, 7)$ are defined by

$$(I_1, I_2, I_3, I_4, I_5, I_7) = \sum_{k=1}^{N} \int_{h_{k-1}}^{h_k} \rho_k (1, Z, Z^2, Z^3, Z^4, Z^6) dZ \tag{A.4}$$

in which ρ_k is the mass density of the kth ply, and

$$\begin{aligned} &\tilde{I}_5' = \hat{I}_3' + \hat{I}_5', \quad \tilde{I}_7 = \hat{I}_7 - \hat{I}_5, \quad \tilde{I}_7' = \hat{I}_7' - \hat{I}_5', \\ &\hat{I}_3 = \bar{I}_4 - \frac{\bar{I}_2 \bar{I}_2}{\bar{I}_1}, \quad \hat{I}_3' = \bar{I}_4' - \frac{\bar{I}_2' \bar{I}_2}{\bar{I}_1'}, \quad \hat{I}_5 = \bar{I}_5 - \frac{\bar{I}_2 \bar{I}_3}{\bar{I}_1}, \\ &\hat{I}_5' = \bar{I}_5' - \frac{\bar{I}_2' \bar{I}_3'}{\bar{I}_1'}, \quad \hat{I}_7 = \frac{\bar{I}_3 \bar{I}_3}{\bar{I}_1} - c_1^2 I_7, \quad \hat{I}_7' = \frac{\bar{I}_3' \bar{I}_3'}{\bar{I}_1'} - c_1^2 I_7, \\ &\bar{I}_1 = I_1 + \frac{2}{R_1} I_2, \quad \bar{I}_2 = I_2 + \frac{1}{R_1} I_3 - c_1 I_4 - \frac{c_1}{R_1} I_5, \\ &\bar{I}_3 = c_1 I_4 + \frac{c_1}{R_1} I_5, \quad \bar{I}_4 = \bar{I}_4' = I_3 - 2c_1 I_5 + c_1^2 I_7, \\ &\bar{I}_5 = \bar{I}_5' = c_1 I_5 - c_1^2 I_7, \quad \bar{I}_1' = I_1 + \frac{2}{R_2} I_2, \\ &\bar{I}_2' = I_2 + \frac{1}{R_2} I_3 - c_1 I_4 - \frac{c_1}{R_2} I_5, \quad \bar{I}_3' = c_1 I_4 + \frac{c_1}{R_2} I_5, \end{aligned} \tag{A.5}$$

in which $c_1 = 4/(3h^2)$.

Appendix B

In Eqs. (14a) and (14b), $[A_{ij}^*]$, $[B_{ij}^*]$, $[D_{ij}^*]$, $[E_{ij}^*]$, $[F_{ij}^*]$ and $[H_{ij}^*]$ are the reduced stiffness matrices determined through relationships [70]

$$\begin{aligned} \mathbf{A}^* &= \mathbf{A}^{-1}, \mathbf{B}^* = -\mathbf{A}^{-1}\mathbf{B}, \mathbf{D}^* = \mathbf{D} - \mathbf{B}\mathbf{A}^{-1}\mathbf{B}, \ \mathbf{E}^* \\ &= -\mathbf{A}^{-1}\mathbf{E}, \ \mathbf{F}^* = \mathbf{F} - \mathbf{E}\mathbf{A}^{-1}\mathbf{B}, \ \mathbf{H}^* = \mathbf{H} - \mathbf{E}\mathbf{A}^{-1}\mathbf{E} \end{aligned} \tag{B.1}$$

where A_{ij} , B_{ij}, D_{ij}, etc., are the panel stiffnesses defined by

$$(A_{ij}, B_{ij}, D_{ij}, E_{ij}, F_{ij}, H_{ij}) = \sum_{k=1}^{N} \int_{h_{k-1}}^{h_k} (\overline{Q}_{ij})_k (1, Z, Z^2, Z^3, Z^4, Z^6) dZ \quad (i, j = 1, 2, 6) \tag{B.2a}$$

$$(A_{ij}, D_{ij}, F_{ij}) = \sum_{k=1}^{N} \int_{h_{k-1}}^{h_k} (\overline{Q}_{ij})_k (1, Z^2, Z^4) dZ \quad (i, j = 4, 5) \tag{B.2b}$$

Appendix C

In Eq. (31)

$$g_{30} = -\left[\gamma_{170} - \left(\gamma_{171} m^2 + \gamma_{172} n^2 \beta^2\right)\right] \tag{C.1}$$

$$
\begin{aligned}
&- \frac{\gamma_{81}m^2 g_{04} + \gamma_{82}n^2\beta^2 g_{03}}{g_{00}} \\
&+ \gamma_{14}\gamma_{24}\frac{g^{\star}_{05}}{g_{06}}\frac{\gamma_{81}m^2 g_{02} + \gamma_{82}n^2\beta^2 g_{01}}{g_{00}} - g^{\star}_{08} \\
&- \gamma_{14}\gamma_{24}\frac{g^{\star}_{07}g^{\star\star}_{05}}{g_{06}},
\end{aligned}
$$

$$
g_{31} = G_{31} - D_{02} + 2G_{32}\Phi(T),
$$

$$
g_{32} = G_{32} - D_{12} + 2G_{33}\Phi(T), \quad g_{33} = G_{33} - D_{22},
$$

in which

$$
G_{31} = g_{08} + \gamma_{14}\gamma_{24}\frac{g^{\star}_{05}g^{\star}_{07}}{g_{06}} + [K_1 + K_2(m^2 + n^2\beta^2)], \quad \text{(C.2)}
$$

$$
\begin{aligned}
G_{32} = &-\frac{2}{3\pi^2 mn}\gamma_{14}\gamma_{24}m^2n^2\beta^2\left(\frac{\gamma_8}{\gamma_6} + \frac{\gamma_9}{\gamma_7} + \frac{1}{4m^2\eta\gamma_6}\right. \\
&\left. + 4\frac{g^{\star}_{05}}{g_{06}}\right)(1 - \cos m\pi)(1 - \cos n\pi)
\end{aligned}
$$

$$
G_{33} = \frac{1}{16}\gamma_{14}\gamma_{24}\left(\frac{m^4}{\gamma_7} + \frac{n^4\beta^4}{\gamma_6}\right),
$$

$$
g^{\star}_{05} = g_{05} + \eta^{-1}(m^2 + \gamma_0 n^2\beta^2),
$$

$$
g^{\star}_{07} = g_{07} + \eta^{-1}(m^2 + \gamma_0 n^2\beta^2),
$$

$$
g^{\star}_{135} = g_{135} + \eta^{-1}(m^2 + 9\gamma_0 n^2\beta^2),
$$

$$
g^{\star}_{315} = g_{315} + \eta^{-1}(9m^2 + \gamma_0 n^2\beta^2),
$$

$$
g^{\star}_{137} = g_{137} + \eta^{-1}(m^2 + 9\gamma_0 n^2\beta^2),
$$

$$
g^{\star}_{317} = g_{317} + \eta^{-1}(9m^2 + \gamma_0 n^2\beta^2),
$$

$$
D_{02} = \gamma_{14}(B_{000}m^2 + b_{000}n^2\beta^2),
$$

$$
D_{12} = \gamma_{14}(B_{100}m^2 + b_{100}n^2\beta^2),
$$

$$
D_{22} = \gamma_{14}(B_{200}m^2 + b_{200}n^2\beta^2),
$$

and other symbols are defined as in Shen [49]. Also

$$
\Phi(T) = \lambda + \Theta_2(\lambda)^2 + \Theta_3(\lambda)^3 + \cdots \quad \text{(C.3)}
$$

where (with m=n=1)

$$
\begin{aligned}
\lambda = &\frac{16}{\pi^2 G_{08}}\left((\gamma_{T3}m^2 + \gamma_{T4}n^2\beta^2)\right. \quad \text{(C.4)} \\
&\left. - \frac{(\gamma_{T3} - \gamma_{T6})m^2 g_{102} + (\gamma_{T4} - \gamma_{T7})n^2\beta^2 g_{101}}{g_{00}}\right)\Delta T \\
&\times \frac{h}{[D^{\star}_{11}D^{\star}_{22}A^{\star}_{11}A^{\star}_{22}]^{1/4}},
\end{aligned}
$$

$$
G_{08} = Q_{11} - D_{02},
$$

$$
\begin{aligned}
\Theta_2 = &\frac{1}{G_{08}}\left[\frac{8}{3\pi^2}\gamma_{14}\gamma_{24}m^2n^2\beta^2\left(\frac{\gamma_8}{\gamma_6} + \frac{\gamma_9}{\gamma_7} + \frac{1}{4m^2\eta\gamma_6}\right.\right. \\
&\left.\left. + 4\frac{g^{\star}_{05}}{g_{06}}\right) - D_{12}\right],
\end{aligned}
$$

$$
\Theta_3 = 2\Theta_2^2 - \frac{g_{33}}{G_{08}},
$$

and for the case of in-plane 'movable' condition

$$
B_{000} = b_{000} = B_{100} = b_{100} = B_{200} = b_{200} = 0, \quad \text{(C.5)}
$$

and for the case of in-plane 'immovable' condition

$$
B_{000} = \eta^{-1}\gamma_{T1}\Delta T, \quad b_{000} = \eta^{-1}\gamma_{T2}\Delta T, \quad \text{(C.6)}
$$

$$
B_{100} = \eta^{-1}\gamma_{24}\frac{\gamma_0 + \gamma_5}{\gamma_{24}^2 - \gamma_5^2}, \quad b_{100} = \eta^{-1}\gamma_{24}\frac{\gamma_{24}^2 + \gamma_0\gamma_5}{\gamma_{24}^2 - \gamma_5^2},
$$

$$
B_{200} = -\frac{1}{8}\gamma_{24}\frac{m^2 + \gamma_5 n^2\beta^2}{\gamma_{24}^2 - \gamma_5^2},
$$

$$
b_{200} = -\frac{1}{8}\gamma_{24}\frac{\gamma_5 m^2 + \gamma_{24}^2 n^2\beta^2}{\gamma_{24}^2 - \gamma_5^2},
$$